Origin of the superconducting state in the collapsed tetragonal phase of KFe_2As_2: Supplemental Information

Daniel Guterding,* Steffen Backes, Harald O. Jeschke, and Roser Valentí
Institut für Theoretische Physik, Goethe-Universität Frankfurt, Max-von-Laue-Straße 1, 60438 Frankfurt am Main, Germany

I. DETAILS OF THE SUSCEPTIBILITY AND PAIRING CALCULATION

For calculating the susceptibility we used $30 \times 30 \times 10$ k-point grids and an inverse temperature of $\beta = 40\ \mathrm{eV}^{-1}$. To calculate the pairing interaction, the susceptibility is needed at k-vectors that do in general not lie on a grid. Those susceptibility values are obtained using trilinear interpolation of the gridded data.

The pairing interaction is constructed using $\sim$ 800 points on the three-dimensional Fermi surface. Consequently, the solution of the gap equation is available only on those points scattered in three-dimensional space. In order to obtain a graphical representation of the gap function on two-dimensional cuts through the Brillouin zone, we used multiscale radial basis function interpolation as implemented in ALGLIB (http://www.alglib.net).

The Hubbard-Hund interaction H_{int} includes the onsite intra (inter) orbital Coulomb interaction U (U'), the Hund's rule coupling J and the pair hopping energy J'. We assume spin rotation-invariant interaction parameters $U = 2.4$ eV, $U' = U/2$, and $J = J' = U/4$. Because of the large bandwidth in the collapsed tetragonal phase, these comparatively large values are necessary to bring the system close to the RPA instability. Note however, that the symmetry of the superconducting gap in this system does not change, even if significantly reduced parameter values are considered.

The parameter values used in the RPA method are renormalized with respect to those in the DFT+DMFT method, because the electronic self-energy is neglected in the usual RPA scheme[1,2].

II. THREE DIMENSIONAL FERMI SURFACE

We extracted the three-dimensional Fermi surface of collapsed tetragonal $CaFe_2As_2$ and KFe_2As_2 from FPLO using $50 \times 50 \times 25$ k-point grids in the two-Fe equivalent Brillouin zone (Fig. 1). For $CaFe_2As_2$ only electron pockets in the Brillouin zone corners are observed. The three-dimensional hole pocket that arises from the bands at M $(\pi, \pi, 0)$ is so small that it is not detected here with the given k-resolution. In KFe_2As_2 one of the hole cylinders is highly dispersive, while the central hole cylinder and the electron pockets located in the corners are nested throughout the entire Brillouin zone.

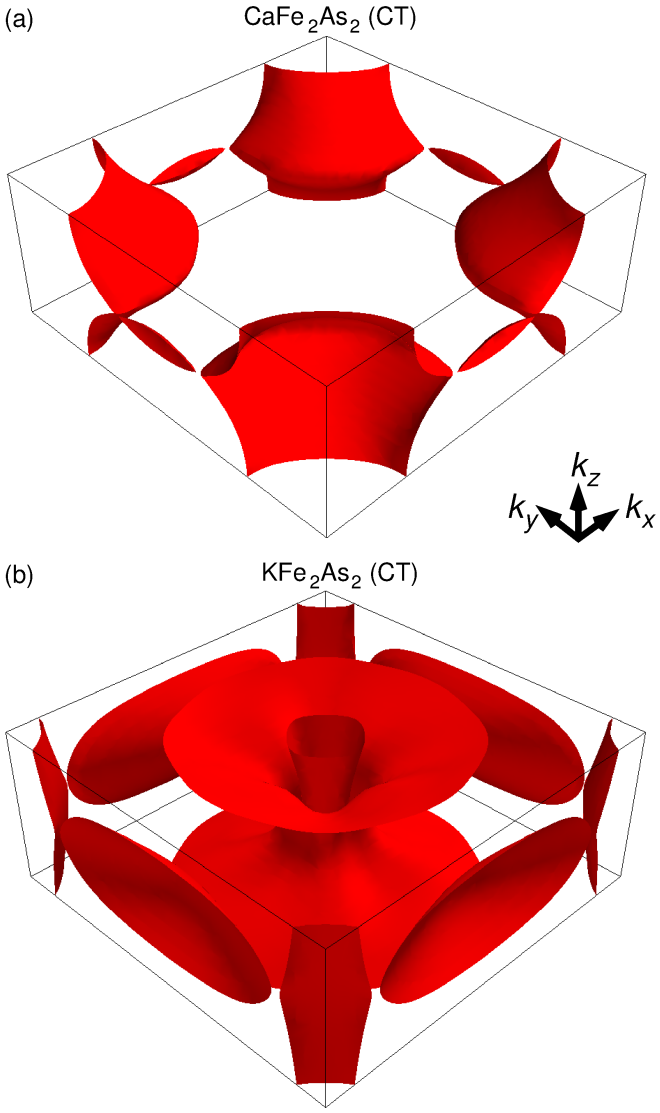

FIG. 1. Three-dimensional Fermi surface of (a) collapsed tetragonal $CaFe_2As_2$ and (b) collapsed tetragonal KFe_2As_2 (both at $P = 21$ GPa) shown in the two-Fe equivalent Brillouin zone. The Γ-point is located in the center of the displayed volume.

III. DFT BANDSTRUCTURE AND FERMI SURFACE OF THE NON-COLLAPSED PHASE UNDER PRESSURE

To verify that electron pockets in KFe_2As_2 do not grow continously with applied pressure, but rather appear as a

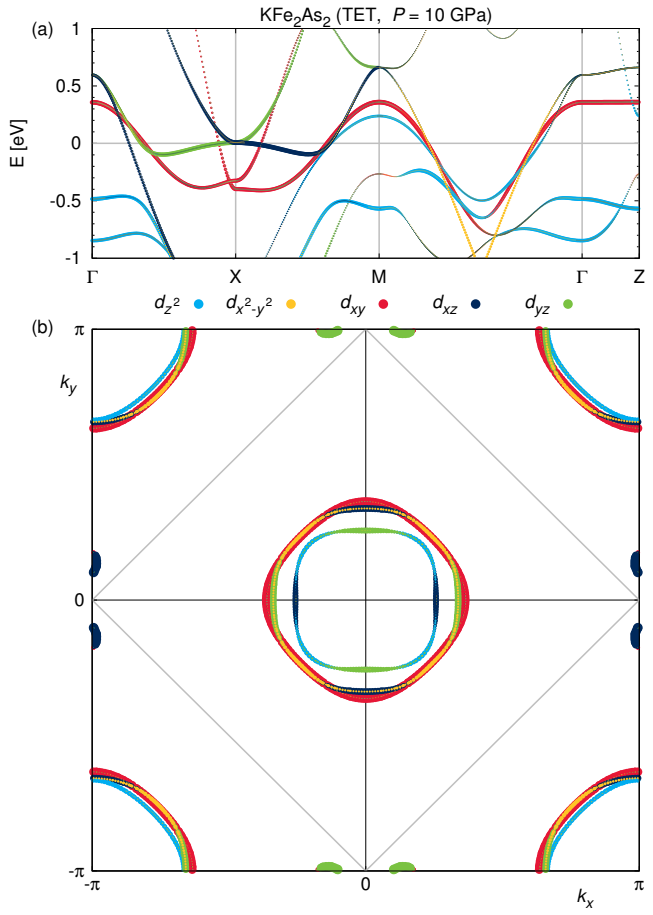

FIG. 2. (a) Electronic bandstructure in the one-Fe equivalent Brillouin zone and (b) Fermi surface of the $P \sim 10$ GPa non-collapsed tetragonal (TET) phase of KFe_2As_2 at $k_z = 0$. The full plot of the Fermi surface spans the one-Fe equivalent Brillouin zone, while the area enclosed by the grey lines is the two-Fe equivalent Brillouin zone. The colors indicate the weights of Fe $3d$ states.

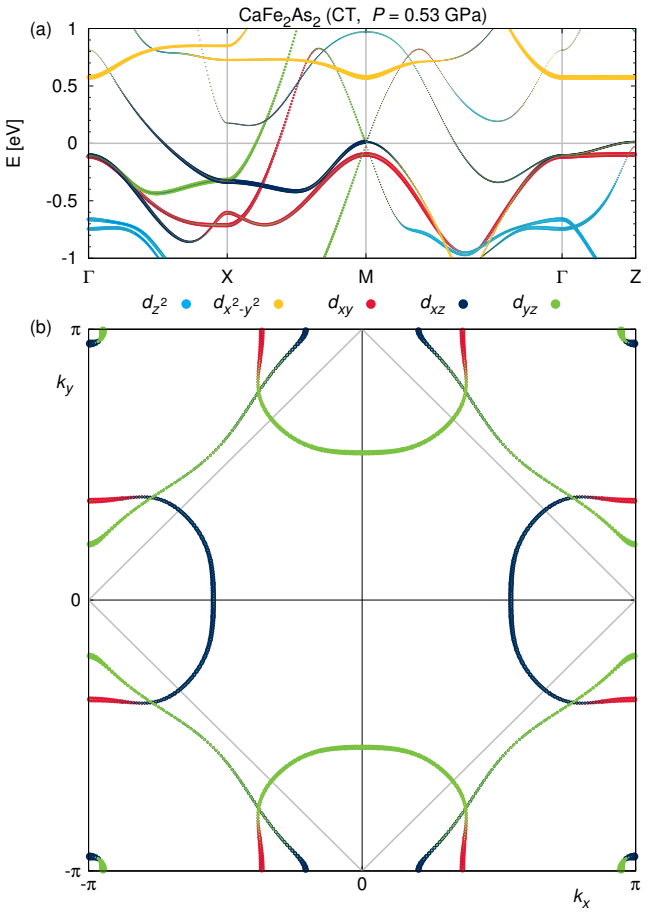

FIG. 3. (a) Electronic bandstructure in the one-Fe equivalent Brillouin zone and (b) Fermi surface of the $P = 0.53$ GPa collapsed tetragonal (CT) phase of $CaFe_2As_2$ at $k_z = 0$. The full plot of the Fermi surface spans the one-Fe equivalent Brillouin zone, while the area enclosed by the grey lines is the two-Fe equivalent Brillouin zone. The colors indicate the weights of Fe $3d$ states.

result of the structural collapse, we have also prepared a crystal structure at $P \sim 10$ GPa, using the data from Ref. 3. The lattice parameters were chosen as $a = 3.663$ Å and $c = 13.0$ Å. The fractional arsenic z-position ($z_{\mathrm{As}} = 0.35750$) was again determined *ab-initio* via structural relaxation using the FPLO code.

No qualitative changes in the bandstructure and Fermi surface (Fig. 2) are observed compared to the ambient pressure structure[4]. Most importantly, electron pockets which are nested with the hole pockets in the Brillouin zone center are not present, even at high pressures slightly below the transition from the tetragonal to the collapsed tetragonal phase. We conclude that the appearance of electron pockets is directly linked to the structural collapse.

IV. BANDSTRUCTURE, FERMI SURFACE AND SUSCEPTIBILITY AT LOW PRESSURES

In the main paper we used crystal structures at $P = 21$ GPa for both materials of interest to ensure that results are comparable. Here we show the electronic bandstructure, Fermi surface and static susceptibility of $CaFe_2As_2$ at low pressure ($P = 0.53$ GPa), right after the structural collapse. We used the experimental structural parameters from Ref. 5, which are the same as in our previous GGA+DMFT study[6]. The differences compared to the high pressure results in the main text are purely quantitative.

The electronic bandstructure and Fermi surface are shown in Fig. 3. The static susceptibility is shown in Fig. 4. The overall enhancement of the susceptibility compared to the figures in the main text is a consequence of the smaller bandwidth at low pressure. The particular enhancement of the peak between X and M in the d_{xz} di-

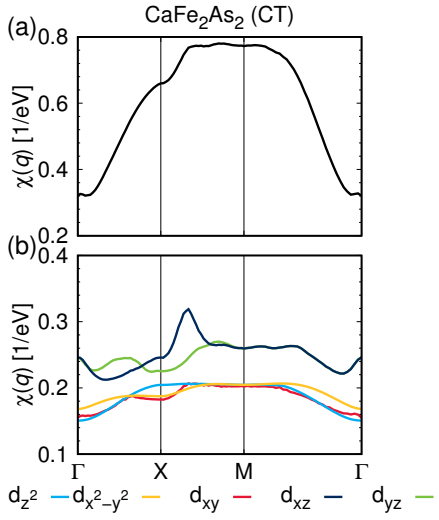

FIG. 4. Summed static susceptibility (a) and its diagonal components χ^{aa}_{aa} (b) in the eight-band tight-binding model for $CaFe_2As_2$ (CT, $P = 0.53$ GPa) in the one-Fe Brillouin zone. The colors identify the Fe $3d$ states.

agonal element of the susceptibility has its origin in the hole band crossing the Fermi level at the M point, which in turn contributes a small three-dimensional pocket.

V. DETAILS OF THE LDA+DMFT CALCULATION

For our DMFT calculations we used a temperature of 290 K, i.e. an inverse temperature $\beta = 40$ eV^{-1}. The interaction parameters are defined in terms of Slater integrals[7] with an on-site Coulomb interaction $U = 4$ eV and Hund's rule coupling $J = 0.8$ eV. As the double counting correction we used the fully localized limit[8,9] (FLL) scheme. Before the continuation of the imaginary-frequency self-energy to the real axis by stochastic analytic continuation[10], the calculation was converged with 2×10^7 Monte-Carlo sweeps for the solution of the impurity model.

From the LDA+DMFT calculation we obtain the spectral function on real frequencies from the analytically continued self-energy as

$$A_{vv'}(k,\omega) = -\frac{1}{\pi}\Im\left[\frac{1}{(\omega+\mu)\delta_{vv'} - \epsilon_{vv'}(k) - \Sigma_{vv'}(k,\omega)}\right], \quad (1)$$

where μ is the chemical potential, $\epsilon_{vv'}(k) = \epsilon_v(k)\delta_{vv'}$ are the eigenenergies of the LDA Hamiltonian and $\Sigma_{vv'}(k,\omega)$ is the impurity self-energy upfolded to Bloch space by projectors $P_{mv}(k)$(see Ref. 11 and 12)

$$\Sigma_{vv'}(k,\omega) = \sum_m P^\dagger_{mv}(k)\left(\Sigma_{mm}(\omega) - \Sigma_{DC}\right)P_{mv'}(k), \quad (2)$$

with the double-counting correction term Σ_{DC} taken in the fully-localized limit (FLL)[8,9]. The diagonal entries

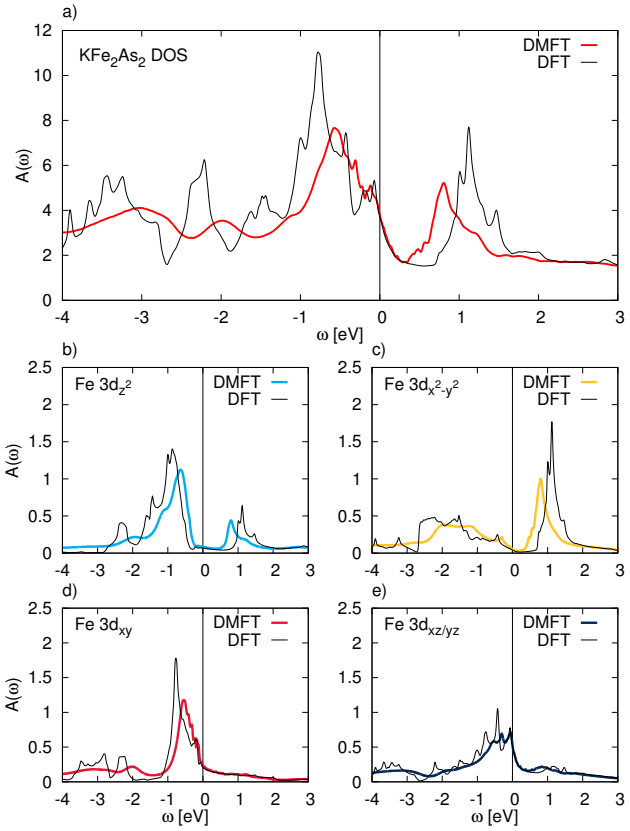

FIG. 5. The k-integrated spectral function (DOS) of KFe_2As_2 at $P = 21$ GPa as obtained within DFT compared to LDA+DMFT. The upper panel (a) shows the total DOS, with the DFT result (black line) and the renormalized LDA+DMFT result (red line). The lower four panels show the partial DOS of the Fe 3d orbitals: (b) $3d_{z^2}$, (c) $3d_{x^2-y^2}$, (d) $3d_{xy}$ and (e) $3d_{xz/yz}$ orbital.

of this object are then integrated over all bands v and k-points k to obtain the total density of states within LDA+DMFT shown in Fig. 5 (a). Additional projection onto the Fe $3d$ orbitals (denoted by index m) by

$$A_{mm'}(k,\omega) = -\frac{1}{\pi}\Im\left[\sum_{vv'} P_{mv}(k)\frac{1}{(\omega+\mu)\delta_{vv'} - \epsilon_{vv'}(k) - \Sigma_{vv'}(k,\omega)}P^\dagger_{m'v'}(k)\right], \quad (3)$$

is then used in the same fashion to obtain the orbital resolved density of states shown in Fig. 5 (b)-(e).

The k-resolved spectral function shown in Fig. 6 was obtained in the same manner, but only integrating over all bands v in order to keep the k-dependence. The orbital resolved Fermi surfaces shown in Fig. 7 and Fig. 8 were obtained by evaluating $A_{mm}(\omega)$ at the Fermi energy ($\omega = \omega_F$) on a 200×200 k-grid in the two-Fe Brillouin zone.

We observe moderate effects of renormalization and broadening in the density of states (see Fig. 5) with

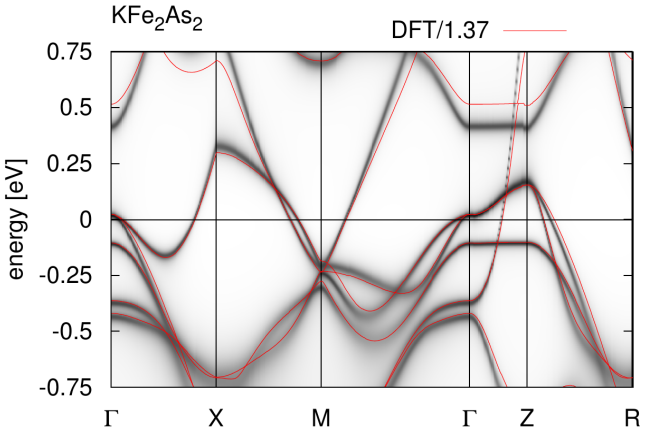

FIG. 6. The k-resolved spectral function of KFe_2As_2 at $P = 21$ GPa as obtained within LDA+DMFT. The red lines show the DFT bandstructure for comparison, rescaled by the average mass enhancement of 1.37. The labels on the x-axis correspond to high-symmetry points in the two-Fe Brillouin zone.

no significant change at the Fermi level. This is confirmed by the k-resolved spectral function (see Fig. 6). Using the FLL double-counting correction, we do not observe any topological changes in the Fermi surface, which closely resembles the DFT result (see Fig. 7 and Fig. 8). However, we observe a closing of the pockets at Γ when the nominal double-counting correction[13] is considered. This indicates that the LDA+DMFT results slightly depend on the double-counting. Note that these changes do not affect our conclusions regarding the superconducting pairing symmetry since only a small fraction of the Brillouin zone around $k_z = 0$ is affected. As the relevant electron-hole nesting takes place around $k_z = \pi$, our superconducting pairing calculations based on the DFT bandstructure should be robust with respect to the effects of correlations.

Note that the Fermi surface plots (Fig. 7 and Fig. 8) have to be rotated by 45° in the plane in order to compare with the Fermi surface plots in the original paper. In 122 compounds the Z-point of the two-Fe Brillouin zone corresponds to the M-point of the one-Fe Brillouin zone.

* guterding@itp.uni-frankfurt.de

[1] S. Graser, T. A. Maier, P. J. Hirschfeld, and D. J. Scalapino, *Near-degeneracy of several pairing channels in multiorbital models for the Fe pnictides*, New J. Phys. **11**, 025016 (2009).

[2] K. Kuroki, H. Usui, S. Onari, R. Arita, and H. Aoki, *Pnictogen height as a possible switch between high-T_c nodeless and low-T_c nodal pairings in the iron-based superconductors*, Phys. Rev. B **79**, 224511 (2009).

[3] J.-J. Ying, L.-Y. Tang, V. V. Struzhkin, H.-K. Mao, A. G. Gavriulik, A.-F. Wang, X.-H. Chen, and X.-J. Chen, *Tripling the critical temperature of KFe_2As_2 by carrier switch*, arXiv:1501.00330 (unpublished).

[4] S. Backes, D. Guterding, H. O. Jeschke, and R. Valentí, *Electronic structure and de Haas-van Alphen frequencies in KFe_2As_2 within LDA+DMFT*, New J. Phys. **16**, 085025 (2014).

[5] A. Kreyssig, M. A. Green, Y. Lee, G. D. Samolyuk, P. Zajdel, J. W. Lynn, S. L. Bud'ko, M. S. Torikachvili, N. Ni, S. Nandi *et al.*, *Pressure-induced volume-collapsed tetragonal phase of $CaFe_2As_2$ as seen via neutron scattering*, Phys. Rev. B **78**, 184517 (2008).

[6] J. Diehl, S. Backes, D. Guterding, H. O. Jeschke, and R. Valentí, *Correlation effects in the tetragonal and collapsed tetragonal phase of $CaFe_2As_2$*, Phys. Rev. B **90**, 085110 (2014).

[7] A. I. Liechtenstein, V. I. Anisimov, and J. Zaanen, *Density-functional theory and strong interactions: Orbital ordering in Mott-Hubbard insulators*, Phys. Rev. B **52**, R5467(R) (1995).

[8] S. L. Dudarev, G. A. Botton, S. Y. Savrasov, C. J. Humphreys, and A. P. Sutton, *Electron-energy-loss spectra and the structural stability of nickel oxide: An LSDA+U study*, Phys. Rev. B **57**, 1505 (1998).

[9] V. I. Anisimov, I. V. Solovyev, M. A. Korotin, M. T. Czyzyk, and G. A. Sawatzky, *Density-functional theory and NiO photoemission spectra*, Phys. Rev. B **48**, 16929 (1993).

[10] K. S. D. Beach, *Identifying the maximum entropy method as a special limit of stochastic analytic continuation*, arXiv:cond-mat/0403055 (unpublished) (2004).

[11] M. Aichhorn, L. Pourovskii, V. Vildosola, M. Ferrero, O. Parcollet, T. Miyake, A. Georges, and S. Biermann, *Dynamical mean-field theory within an augmented plane-wave framework: Assessing electronic correlations in the iron pnictide LaFeAsO*, Phys. Rev. B **80**, 085101 (2009).

[12] J. Ferber, K. Foyevtsova, H. O. Jeschke, and R. Valentí, *Unveiling the microscopic nature of correlated organic conductors: The case of κ-$(ET)_2Cu[N(CN)_2]Br_xCl_{1-x}$*, Phys. Rev. B **89**, 205106 (2014).

[13] K. Haule, *Exact double-counting in combining the Dynamical Mean Field Theory and the Density Functional Theory*, arXiv:1501.03438 (unpublished).

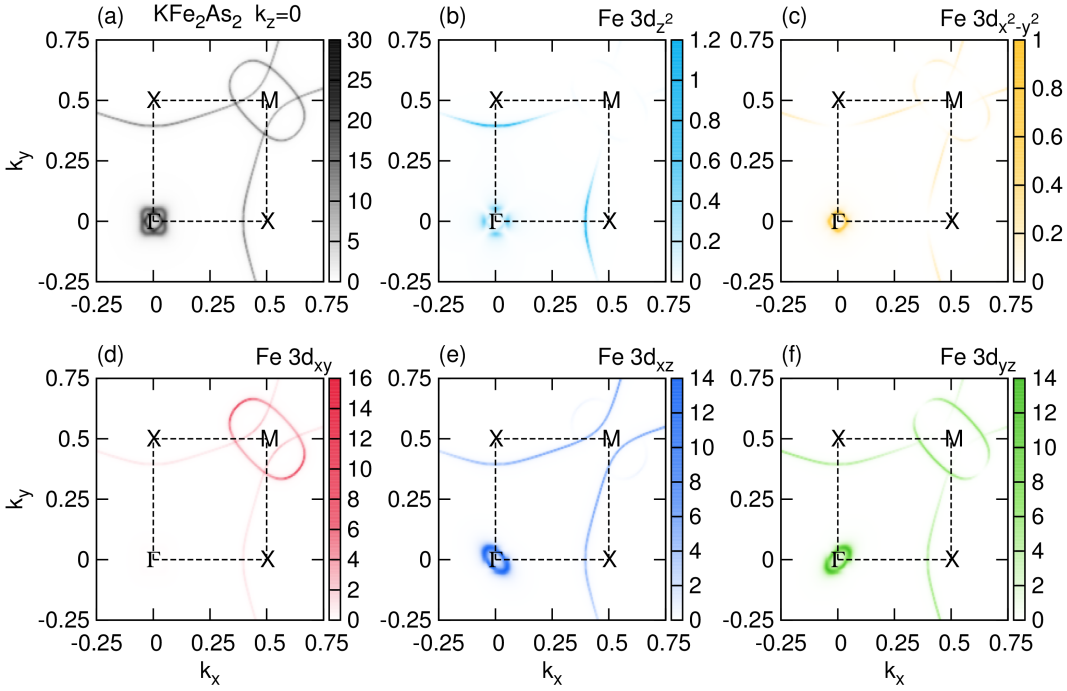

FIG. 7. The $k_z = 0$ Fermi surface of KFe_2As_2 at $P = 21$ GPa as obtained within LDA+DMFT in the two-Fe Brillouin zone. Panel (a) shows the total spectral function, while panels (b)-(f) show the orbital resolved spectral function for the Fe $3d$ orbitals.

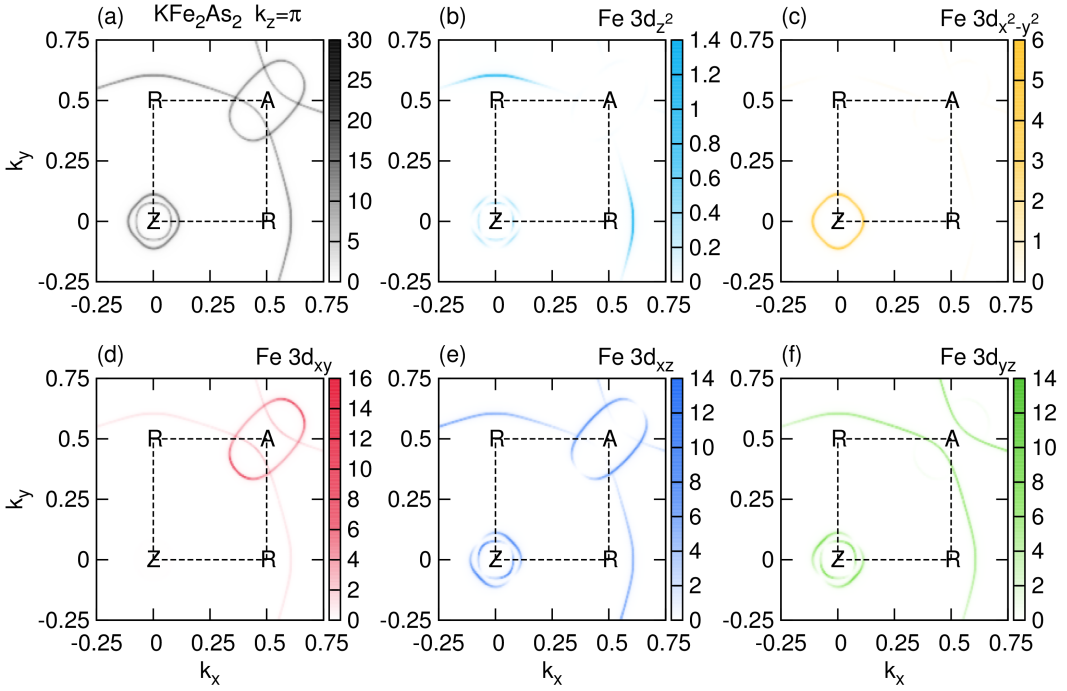

FIG. 8. The $k_z = \pi$ Fermi surface of KFe_2As_2 at $P = 21$ GPa as obtained within LDA+DMFT in the two-Fe Brillouin zone. Panel (a) shows the total spectral function, while panels (b)-(f) show the orbital resolved spectral function for the Fe $3d$ orbitals.